Materials International
Open Access Journal (ISSN: 2668-5728)

Article
Volume 7, Issue 1, 2025, 2
https://doi.org/10.33263/Materials71.002

Theoretical Evaluation of Urea Derivatives on Fe (110) and Sn (111) Surfaces: DFT and Monte Carlo Simulation Approaches

Terngu Timothy Uzah [1,*]

[1] Department of Chemistry, College of Science, Federal University of Petroleum Resources, Effurun, Nigeria; uzah2t@gmail.com;
* Correspondence: uzah2t@gmail.com;

Scopus Author ID 57207466454
Received: 11.07.2024; Accepted: 6.10.2024; Published: 6.01.2025

Abstract: Present-day theoretical computation methods are quite effective at anticipating how corrosion inhibitors would behave on metal surfaces, conserving time and resources on laboratory testing. The present study aims to predict the inhibitory effectiveness of certain furan derivatives on surfaces of Fe (110) and Sn (111) in acidic media. To compare their fundamental attributes against corrosion as well as their behavior on iron (Fe) and tin (Sn) surfaces in an acid medium, six urea derivatives have been chosen for this purpose: Imidazolidin-2-one (Cpd A), 4-methylimidazolidine-2-one (Cpd B), Tetrahyropyrimidin-2(1H)-one (Cpd C), 1,3-dimethylimidazolidin-2-one (Cpd D), 1,1-diethylurea (Cpd E), 1,3-dimethylurea (Cpd F). The anti-corrosive characteristics of Cpds A - F were generally explored using Density Functional Theory and Monte Carlo simulations. The results indicate that the compounds had low energy gaps, the highest occupied molecular orbital energy, global hardness, as well as ionization energy and high Electron affinity, E_{LUMO}, global softness, and number of transferred electrons, which explained their corrosion inhibition potentials. Electrostatic potential (ESP) and Fukui indices identified the reactive sites with the ability to accept and donate electrons via back-donation to the metal's d-orbital. The Monte Carlo simulation demonstrated a favorable contact between the Fe (110) and Sn (111) surfaces and inhibitory molecules in the acidic medium. In the industrial sectors, these compounds may be secured as corrosion protectors.

Keywords: tin; DFT; Fukui indices; energy gap; MC simulation; urea derivatives.

1. Introduction

Corrosion is a significant problem for the industry because this metal and its alloys are used in so many distinct fields; even though this metal resists corrosion in some chemical conditions and the atmosphere, it can still deteriorate when oxygen and other aggressive anions are present, especially in acidic media. However, it can be hard to anticipate, identify, and guard against corrosion [1,2]. As a result, the topic of metal corrosion avoidance has received a lot of interest due to the extensive usage of metals and their alloys in various industries, leading to several completed and ongoing studies [3]. The best and least expensive method of controlling metal corrosion in acidic conditions is to use corrosion inhibitors. The preferred corrosion inhibitors for metal were chromates, molybdates, and tetraborates; nevertheless, their application was beset by difficulties due to toxicity, low efficacy, and instability of the protective film [4]. On the other hand, due to their strong corrosion inhibition, organic adsorption inhibitors like urea and its derivatives were more effective at shielding metal. The molecular structure of these corrosion inhibitors consists of heteroatoms such as N, O, P, and S, which act as adsorption centers and promote adsorption on the metal surface [5-7].

The inhibitory impact of corrosion inhibitors is assessed using a variety of chemical, electrochemical, and surface morphological approaches [8]. These practical techniques do, however, have a few drawbacks. These practical techniques are typically linked to costly synthesis and the use of hazardous chemicals that harm the environment [9,10]. Toxic and costly starting ingredients and catalysts are used in multistep reactions to create these compounds, which require enormous volumes of solvents for the purification and work-up stages. Serious environmental problems arise when hazardous catalysts and excess organic solvents are released. Corrosion inhibitor synthesis is a multistep process that might result in the development of various unwanted side products and environmental pollution. Despite their extremely costly and poisonous manufacture, most of the chemicals do not produce positive outcomes and are unsuccessful in experiments. [11-13]. Computational software is currently gaining popularity as a reliable resource for explaining how corrosion inhibitors behave in various environments and on metal surfaces [14-17]. A computational modeling technique called density functional theory (DFT) is typically employed to look at the inherent characteristics of molecules. Predicting an inhibitor's chemical properties, such as its energy gap between the highest and lowest occupied molecular orbitals (HOMO–LUMO), chemical hardness, softness, electronegativity, chemical potential, electrophilicity, and nucleophilicity of its constituent chemical species, is the primary goal of this research.

In contrast, the action of the inhibitors on the metal surfaces was studied using Monte Carlo simulations. Calculations and studies are done on binding and adsorption energies [18,19]. The present study examined six urea derivatives (Figure 1) in an acidic medium to determine their suitability as effective corrosion inhibitors on the surfaces of Fe (110)) and Sn (111). Various theoretical approaches, including density functional theory (DFT) and Monte Carlo (MC) simulation techniques, were used to evaluate the inherent characteristics of the chosen inhibitors to complement this theoretical study.

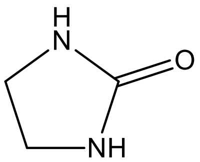

imidazolidin-2-one (Cpd A)

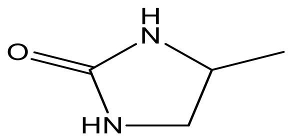

4-methylimidazolidin-2-one (Cpd B)

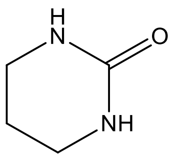

tetrahydropyrimidin-2(1*H*)-one (Cpd C)

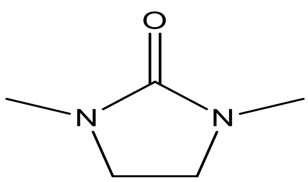

1,3-dimethylimidazolidin-2-one (Cpd D)

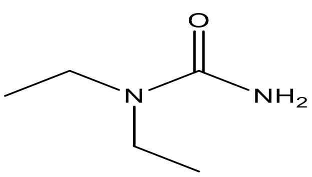

1,1-diethylurea (Cpd E)

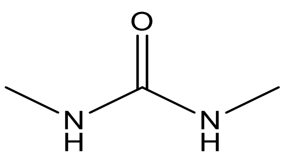

1,3-dimethylurea (Cpd F)

Figure 1. Structures of the urea derivatives (Cpds A-F).

2. Computational Details

2.1. Quantum chemical calculations.

The Gaussian 09W package was utilized to accomplish the theoretical analyses. For all molecules, a complete optimization was carried out using the 6-311G+ (d,p) basis set, which is well-recognized for providing precise geometries and electrical characteristics for various organic compounds. DFT/B3LYP methods with 6-311G+ (d,p) basis set in the gas phase were used to perform quantum chemical calculations about the examined inhibitors. By using the following equations, (Koopmann's theorem determines) energy gap (ΔE), dipole moment (μ), global electronegativity (χ), global softness (σ), chemical hardness (η), the fractions of electrons transferred (ΔN), ionization potential (I) and electron affinity (A). E_{HOMO}, E_{LUMO}, and ESP maps were plotted [20,21].

$$\text{Electron affinity } (A) = E_{LUMO} \quad (1)$$

$$\text{Ionization potential } (I) = E_{HOMO} \quad (2)$$

$$\text{Energy gap } (\Delta E) = E_{LUMO} - E_{HOMO} \quad (3)$$

$$\text{chemical hardness } (\eta) = (\frac{\delta^2 E}{\delta N^2})_v = (\frac{\delta \mu}{\delta N})_v = \frac{\Delta E}{2} \quad (4)$$

$$\text{Global softness } (\sigma) = 2(\frac{\delta N}{\delta \mu})_{v(r)} = \frac{1}{\eta} = \frac{2}{\Delta E} \quad (5)$$

$$\text{Global electronegativity } (\chi) = \frac{-(E_{HOMO} + E_{LUMO})}{2} \quad (6)$$

$$\text{Fractions of electrons transferred } (\Delta N) = \frac{(\chi_{metal} - \chi_{inh})}{2 \times (\eta_{metal} - \eta_{inh})} \quad (7)$$

Where, E_{HOMO}= highest occupied molecular orbital's energy, E_{LUMO}= lowest unoccupied molecular orbital, ΔE = energy gap, μ = dipole moment, χ = global electronegativity, σ = global softness, η = chemical hardness, and ΔN = fractions of electrons transferred, χ_{meta} (χ_{Fe} = 4.82 eV χ_{Sn} = 4.42 eV) and χ_{inh}= absolute electronegativities of the metal and organic inhibitor, respectively. η_{metal} (η_{Fe} = η_{Sn} = 0 eV) and η_{inh} = absolute hardness of the metal and organic inhibitor, respectively [22,23]

2.2. The Fukui function analysis.

Utilizing the Dmol3 computation via Material Studio, we have employed the condensed Fukui function via finite difference approximation from Mulliken population analysis to interpret both electrophilic and nucleophilic reactive centers on the studied inhibitors. The following is how the Fukui functions were found [24].

2.3. Monte Carlo simulation.

The BIOVIA material studio application was used to create the adsorption model for inhibitor (Cpd A - F) on the (110) and (111) planes of Fe and Sn, respectively. Based on earlier research that revealed the Fe (110) and Sn (111) planes to have a highly packed structure and a high stabilization energy [25], these planes are chosen as the metal substrate. Using the Material Studio's builder module, the crystal structure of Fe and Sn were created. The Fe and Sn crystals broke along the (110) and (111) planes, respectively. Then, the surfaces were increased to 10 × 10 supercells, which were made to maximize the amount of water and inhibitor that could interact with the Fe and Sn surfaces. A 30Å thick vacuum slab was constructed. The Condensed-phase Optimized Molecular Potentials for Atomistic Simulation Studies COMPASS Force field was used to minimize energy to relax the Fe (110) and Sn (111) surfaces [26,27]. The Fe (110) and Sn (111) surface was exposed to a single optimized inhibitor molecule in the gas phase. The adsorption locator module was then used to introduce 500 water molecules and inhibitors.

3. Results and Discussion

3.1. Quantum chemical calculations.

Figure 2 shows the compounds with molecular orbitals optimized geometry and EHOMO and ELUMO in Figure 3. ΔE, χ, σ, η, ω, ΔN, I, A, EHOMO, and ELUMO are the quantum chemical parameters that were determined for the inhibitors using the B3LYP/6-31+ (d,p) method. as listed in Table 1.

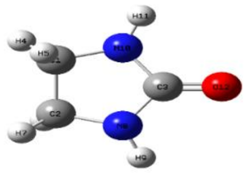

Cpd A

Cpd B

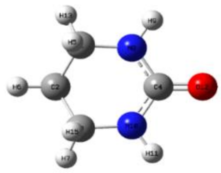

Cpd C

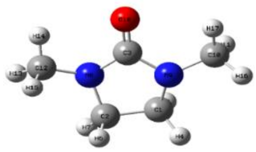

Cpd D

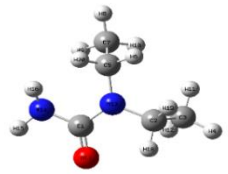

Cpd E

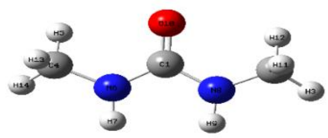

Cpd F

Figure 2. The Optimized Structures of inhibitor molecules (Cpd A-F) using the B3LYP/6-31+ (d,p).

Table 1. Quantum chemical data for molecules under study.

Compound	Cpd A	Cpd B	Cpd C	Cpd D	Cpd E	Cpd F
E_{LUMO}	-0.00716	-0.00950	-0.01004	-0.00166	-0.01265	-0.00886
E_{HOMO}	-0.26183	-0.25906	-0.25206	-0.23750	-0.24554	-0.2430
μ	4.613	4.706	4.929	4.118	4.113	4.072
ΔE	0.2546	0.2496	0.2406	0.2358	0.2328	0.2341
η	0.1273	0.1248	0.1203	0.1179	0.1164	0.1171
σ	7.855	8.013	8.313	8.482	8.591	8.543
χ	0.1345	0.1343	0.1311	0.1196	0.1291	0.1259
ΔN_{Fe}	-18.40	-18.77	-19.47	-19.93	-20.15	-20.04
ΔN_{Sn}	-16.83	-17.17	-17.81	-18.24	-18.43	-18.34

Higher EHOMO values indicate a strong inclination for the molecules to donate electrons to the metal surface's d orbital, but lower ELUMO values indicate a superior ability to accept electrons through back donation.

The inhibitor-metal complex's stability can be inferred from the energy gap (ΔE) that exists between the ELUMO and EHOMO. The inhibitors are firmly adsorbed on the surface of metals when the ΔE value is lower, indicating that the compounds may easily donate their electrons to the metal's d orbital [28]. A small energy gap is indicative of an effective inhibitor because ΔE is a crucial characteristic that indicates the reactivity of the inhibitor molecule [29]. The order of all ΔE values for the inhibitors examined is Cpd E > Cpd F > Cpd D > Cpd C > Cpd B > Cpd A, indicating that Cpd E has a good level of inhibitory potency in comparison to the rest of the compounds (Tables 1).

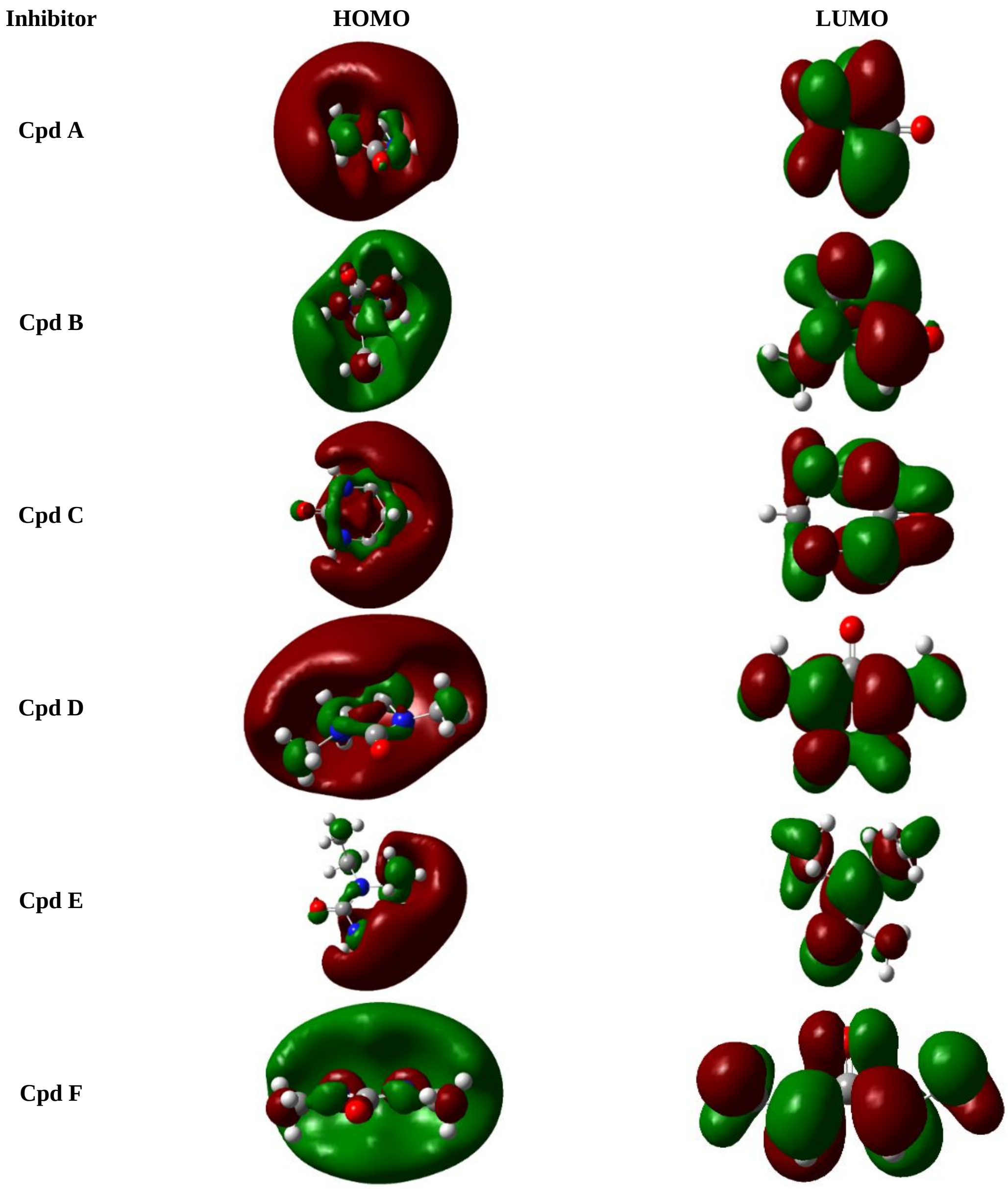

Figure 3. The highest occupied molecular orbitals (HOMOs) and lowest unoccupied molecular orbitals (LUMOs) of inhibitor molecules using B3LYP/6-31+ (d,p).

Global electronegativity (χ) from ELUMO and EHOMO can be used to estimate the reactivity of the inhibitors. This estimation is contingent upon the findings indicating that Cpd E has a lower electronegativity value than Cpd F and Cpds A - D. Cpd E thus tends to react more as an electron donor when it comes to the reactivity of these compounds [30, 31].

The global hardness and softness values are remarkably arranged as follows: Cpd E > Cpd F > Cpd D > Cpd C > Cpd B > Cpd A. This indicates that Cpd E is more reactive than Cpd F and Cpds A - D (Table 1). This is because it has been shown that an atom's resistance to a charge transfer, or the screened interaction energy of the electrons in the frontier (HOMO and LUMO) orbitals, is exactly what determines a molecule's chemical hardness or softness

[32]. Therefore, a low global hardness value or a high global softness value will probably exhibit a high inhibitory efficiency.

Table 1 also indicates that ΔN for Cpds A - F agrees with all adopted bases in addition to the number of electrons transferred, which states that for an inhibitor to be effective, ΔN must be less than 3.6 (electrons) [24]. Cpd E is predicted to have the highest inhibition performance compared to the other examined inhibitors. The dipole moment (μ) in all the tested compounds in Debye is greater than water's μ (1.85 Debye), indicating that the molecule has a considerable propensity to adsorb on the metal surface by substituting pre-adsorbed water molecules [28].

3.2. Electrostatic potential maps (ESP).

Electrostatic potential maps, or ESP maps related to nucleophilic and electrophilic activity sites in molecules, were employed to visualize the electron density at various locations and identify the more reactive centers in the inhibitor molecule. The ESP map (Figure 4) displays the region with the highest negative electrostatic potential as red and yellow, the region with the highest positive electrostatic potential as blue, and the region with the lowest electrostatic potential as green [33]. Therefore, it makes reasonable sense to consider that the urea derivatives inhibitors contain several adsorption sites, which are distinguished from each other predominantly by the N and O atoms.

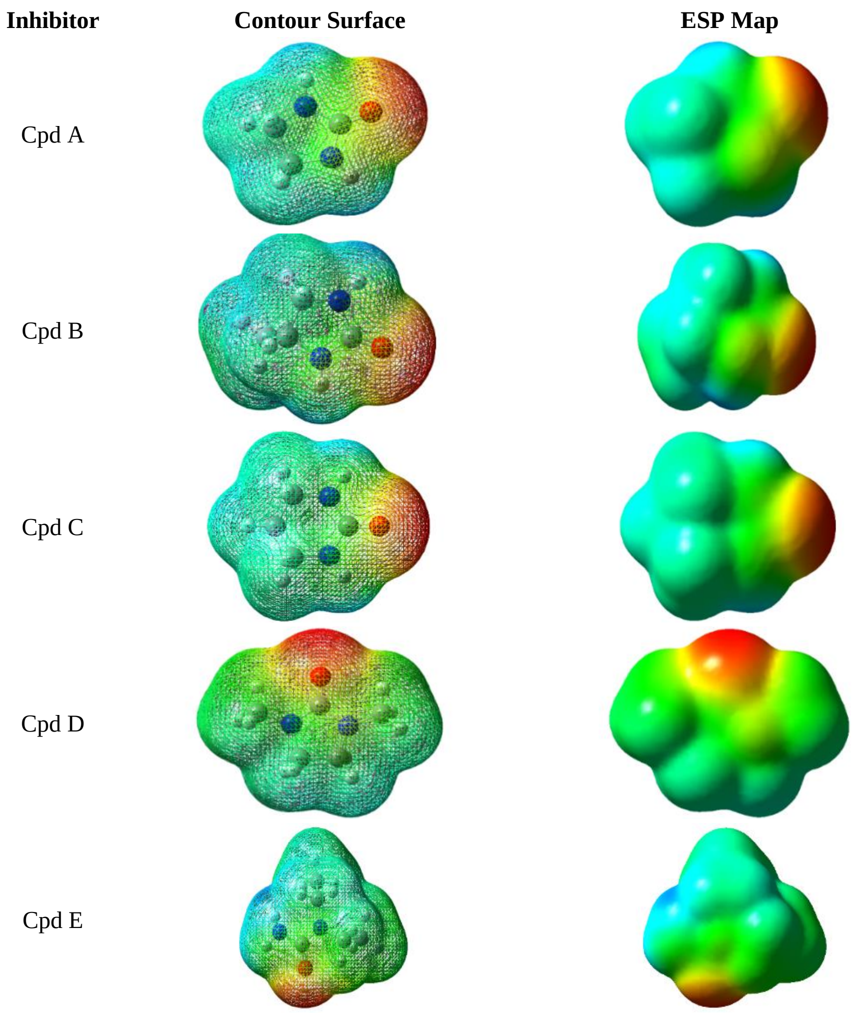

Cpd F 

Figure 4. The contour (left) and ESP (right) map representation of electrostatic potential regions for inhibitor molecules using the B3LYP/6-31+ (d,p).

3.3. Fukui indices.

Fukui calculations are helpful in assessing a molecule's reactive centers against electrophilic and nucleophilic attacks. Table 2 displays the electron density of the Fukui indices. $f_a^-$and f_a^+ derived from Mulliken population analysis in addition to the Fukui values. The highest value of f_a^+For oxygen it comes from Mulliken population analysis, indicating the strongest nucleophilicity of the atom and its ability to receive an electron from the metal surfaces [24,26]. These atoms are found on O (6), N (1,4), O (7), O (6), O (4), and O (4) for Cpds A - F respectively. The oxygen atom's propensity to transfer electrons to the metal surface in examined inhibitors is revealed by the greatest value of f_a^-. (-0.485, -0.563, -0.481, -0.492, -0.498, and -0.494 for Cpds A - F, respectively) are the more reactive sites for electrophilic attack, according to the parameters of local reactivity descriptors.

Table 2. Fukui function indices of O, N, and C atoms of the molecules calculated at the B3LYP/6-31G+ (d,p).

Atom	f_a^-	f_a^+	Δf_a		f_a^-	f_a^+	Δf_a
	Cpd A				Cpd F		
C1	0.061	0.075	0.014	N1	-0.421	-0.423	-0.02
C2	0.061	0.075	0.014	C2	0.626	0.622	-0.004
N3	-0.401	-0.406	-0.005	N3	-0.426	-0.418	0.008
C4	0.608	0.607	0.001	O4	-0.494	-0.519	-0.025
N5	-0.401	-0.407	-0.006	C5	0.019	0.028	0.009
O6	-0.485	-0.504	-0.019	C6	0.038	0.047	0.009
	Cpd B				Cpd C		
N1	-0.563	-0.573	-0.01	N1	-0.404	-0.410	0.006
C2	0.023	0.030	0.007	C2	0.056	0.072	0.016
C3	-0.113	-0.107	0.006	C3	-0.122	-0.108	0.014
N4	-0.561	-0.573	-0.012	C4	0.077	0.090	0.018
C5	0.678	0.647	-0.031	N5	-0.410	-0.415	-0.005
O6	-0.466	-0.524	-0.058	C6	0.606	0.589	-0.017
C7	-0.409	-0.405	0.004	O7	-0.481	-0.526	-0.045
	Cpd D				Cpd E		
N1	-0.449	-0.460	-0.011	N1	-0.406	-0.401	0.005
C2	0.064	0.072	0.008	C2	0.614	0.606	-0.008
C3	0.060	0.069	0.009	N3	-0.438	-0.456	-0.018
N4	-0.453	-0.464	-0.011	O4	-0.498	-0.527	-0.028
C5	0.644	0.619	-0.025	C5	0.055	0.066	0.011
O6	-0.492	-0.519	-0.027	C6	0.040	0.057	0.017
C7	0.024	0.034	0.01	C7	-0.134	-0.130	0.004
C8	0.023	0.031	0.008	C8	-0.133	-0.127	0.006

3.4. Monte Carlo simulations.

On the Fe (110) and Sn (111) surfaces, Monte Carlo simulations were used to study the adsorption characteristics of the tested urea derivatives. Figures 5 and 6 illustrate how compounds might be adsorbed on the Fe (110) and Sn (111) surfaces via two different viewpoints, allowing one to see the equilibrium adsorption configuration of the studied molecules on the metals’ surfaces. The inhibitor molecules were observed to be parallel on the

Fe (110) surface and quasi-parallel on the Sn (111) surface when viewed from the side perspective. All molecules are flat on the metal surfaces when viewed from above. Table 3 shows the sequence of adsorption energies for all molecules on Fe (110) and Table 4 on Sn (111) surfaces. The adsorption energy of Cpd E in the case of Fe (110) is the lowest, at -13177 kcal mol. For the Sn (111) surface, the values for Cpd C and Cpd D (-24.283 and -45.026 kcal mol, respectively) were the lowest. As indicated by all values, the compound's adsorption on the metal surfaces is thermodynamically stabilized, with Cpd E being the most stable and readily adsorbed [34- 36]. One adsorbate (water) component removed from a metal adsorbate configuration is often represented by the energy of the substrate-adsorbate configuration (dEads/dNi). Generally speaking, the greater the inhibitor-metal component interaction, the lower the value of dEads/dNi. [21,28,37]. Cpd E > Cpd F > Cpd D > Cpd C > Cpd B > Cpd A is the order of the dEads/dNi for both Fe (110) and Sn (111) surfaces.

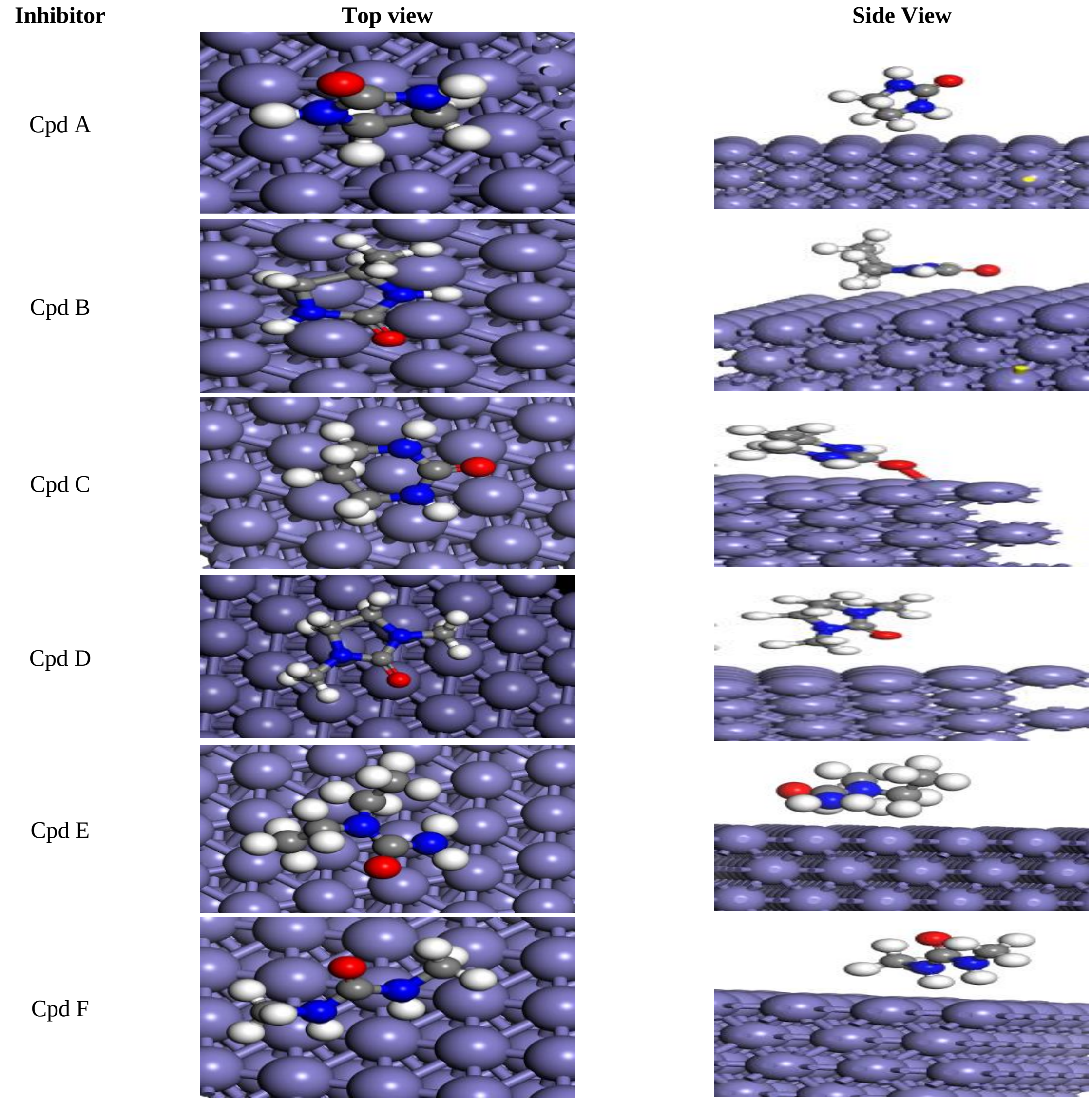

Figure 5. Top view (left) and Side view (right) of the urea derivatives (Cpds A-F) on the Fe (110) Surface.

Table 3. Monte Carlo simulation parameters of adsorption of the tested urea derivative molecules on Fe (110) surface.

Compound (Fe (110))	dEad/dNi	Adsorption energy	Rigid adsorption energy	Deformation energy	Total energy
Cpd A	-14.721	-42.640	-10.467	-32.1729	18.275
Cpd B	-15.611	-30.085	-5.0316	-25.053	32.593
Cpd C	-28.342	-75.319	-21.731	-53.587	16.678

Compound (Fe (110))	dEad/dNi	Adsorption energy	Rigid adsorption energy	Deformation energy	Total energy
Cpd D	-28.425	-67.433	-13.664	-53.769	55.133
Cpd E	-658846	-13177	-5.3668	-1317684	9.5122
Cpd F	-34.142	-59.158	-5.1689	-53.989	34.917

Inhibitor **Top view** **Side View**

Cpd A

Cpd B

Cpd C

Cpd D

Cpd E

Cpd F

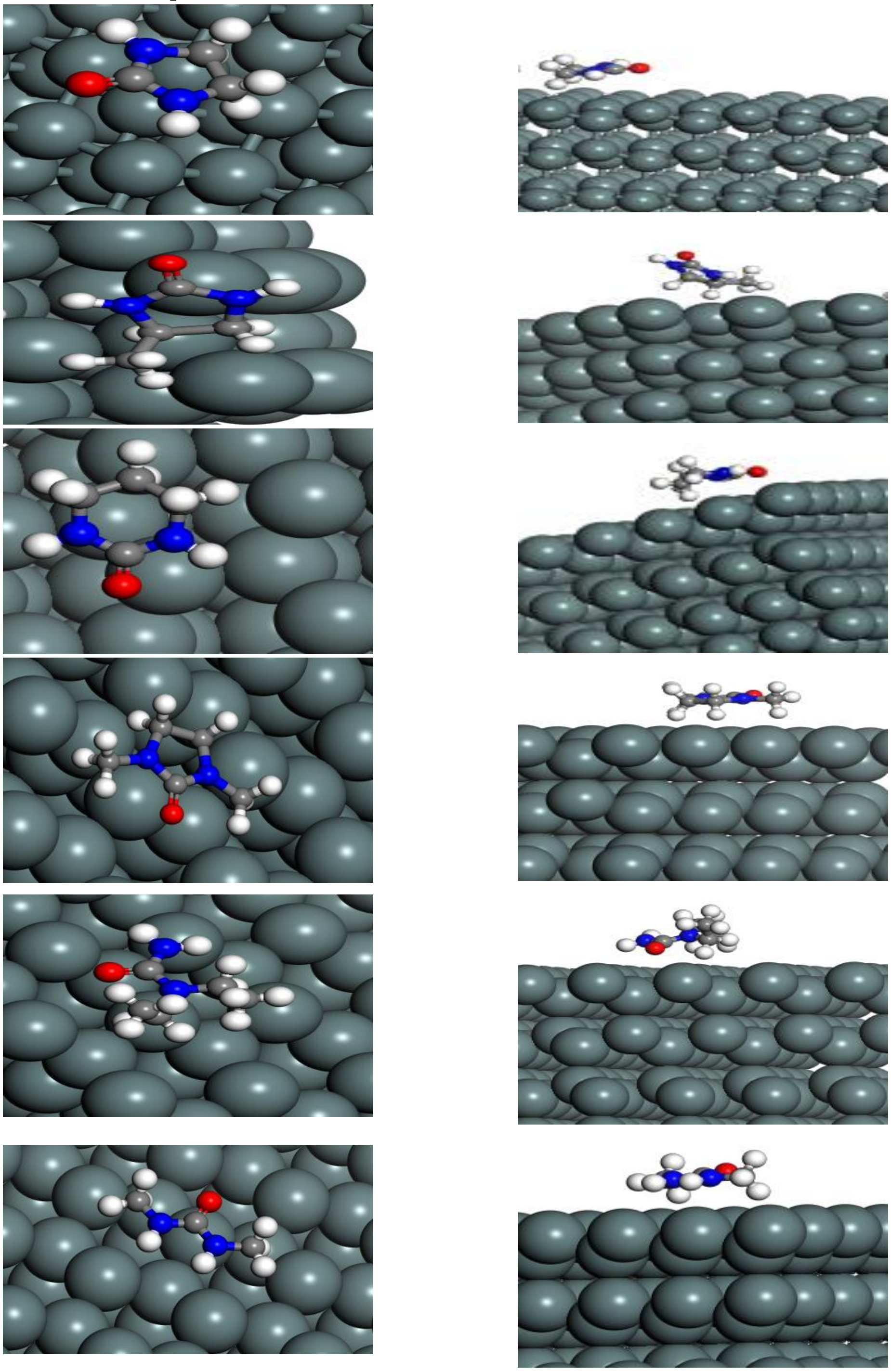

Figure 6. Top view (left) and Side view (right) of the urea derivatives (Cpd A-F) on the Sn (111) Surface.

Table 4. Monte Carlo simulation parameters of adsorption of the tested urea derivative molecules on Sn (111) surface.

Compound (Sn (111))	dEad/dNi	Adsorption energy	Rigid adsorption energy	Deformation energy	Total energy
Cpd A	-4.9134	-65.829	-32.1018	-22.918	-20.889
Cpd B	-21.351	-45.026	-19.979	-25.047	17.653
Cpd C	-24.283	-24.283	-12.333	-11.949	11.627

Compound (Sn (111))	dEad/dNi	Adsorption energy	Rigid adsorption energy	Deformation energy	Total energy
Cpd D	-32.234	-63.493	-27.409	-36.084	-1.869
Cpd E	-65885	-13177	-22.459	-13177	-7.708
Cpd F	-39.320	-116.76	-33.846	-38.401	26.442

4. Conclusions

Six urea derivatives — Imidazolidin-2-one (Cpd A), 4-methylimidazolidine-2-one (Cpd B), Tetrahyropyrimidin-2(1H)-one (Cpd C), 1,3-dimethylimidazolidin-2-one (Cpd D), 1,1-diethylurea (Cpd E), 1,3-dimethylurea (Cpd F) were compared. Their corrosion inhibition efficiencies were assessed using DFT calculations and Monte Carlo simulations through various basis sets on Fe (110) and Sn (111) surfaces. The HOMO and LUMO maps revealed the asymmetric distribution of charge. The Fukui local reactivity indices and the electrostatic potential (ESP) maps revealed that the N and O atoms comprise most of the reactive sites in inhibitors Cpd A-F. The efficacy of urea derivatives, Cpd A-F against Fe (110) and Sn (111) surface corrosion can be ascertained by combining the adsorption energy and the desorption energy (dEads/dNi) values. Based on DFT and MC simulations, the sequence of these inhibitors' effectiveness is Cpd E > Cpd F > Cpd D > Cpd C > Cpd B > Cpd A.

Funding

This research received no external funding.

Acknowledgments

The author would like to acknowledge the Federal University of Petroleum Resources, Effurun, for creating an enabling environment for this research work.

Conflicts of Interest

The author declares no conflict of interest.

References

1. King, D.; World Economic, F. The Future of Industrial Biorefineries; World Economic Forum: **2010**.
2. Shaw, B.A.; Kelly, R.G. What is Corrosion? *Electrochem. Soc. Interface* **2006**, *15*, 24–27.
3. Bashir, S.; Sharma, V.; Dhaundiyal, P.; Shafi, N.; Kumar, A. Gymneme Sylvestre as a green corrosion inhibitor for aluminum in an acidic medium. *Port. Electrochim. Acta* **2021**, *39*, 199–212, https://doi.org/10.1080/00986445.2020.1752680.
4. Zadeh, F. M. H.; Khaleghi, M.; Bordbar, S.; Jafari, A. Myrtus communis extract: a bio-controller for microbial corrosion induced by sulphate reducing bacteria. *Corros. Eng. Sci. Technol.* **2021**, *56*, 269–278, http://dx.doi.org/10.1080/1478422X.2020.1850401.
5. Sharma, S.; Ganjoo, R.; Kr. Saha, S.; Kang, N.; Thakur, A.; Assad, H.; Sharma, V.; Kumar, A. Experimental and theoretical analysis of baclofen as a potential corrosion inhibitor for mild steel surface in HCl medium. *J. Adhes. Sci. Technol.* **2021**, 1–26, http://dx.doi.org/10.1080/01694243.2021.2000230.
6. Thakur, A.; Kumar, A.; Kaya, S.; Vo, D. V. N.; Sharma, A. Suppressing inhibitory compounds by nanomaterials for highly efficient biofuel production: A review. *Fuel* **2022**, *312*, 122934, http://dx.doi.org/10.1016/j.fuel.2021.122934.
7. Sharma, S.; Ganjoo, R.; Kr. Saha, S.; Kang, N.; Thakur, A.; Assad, H.; Kumar, A. Investigation of inhibitive performance of Betahistine dihydrochloride on mild steel in 1 M HCl solution. *J. Mol. Liq.* **2022**, *347*, 118383, https://doi.org/10.1016/j.molliq.2021.118383.

8. Chen, L.; Lu, D.; Zhang, Y. Organic Compounds as Corrosion Inhibitors for Carbon Steel in HCl Solution: A Comprehensive Review. *Materials* **2022**, *15*, 2023, https://doi.org/10.3390/ma15062023.
9. Yadav, D. K.; Quraishi, M. A. Application of some condensed uracils as corrosion inhibitors for mild steel: gravimetric, electrochemical, surfacemorphological, UV–visible, and theoretical investigations. *Ind. Eng. Chem. Res.* **2012**, *51*, 14966–14979, http://dx.doi.org/10.1021/ie301840y.
10. Chigondo M.; Chigondo, F. Recent natural corrosion inhibitors for mild steel: an overview, *J. Chem.* **2016**, 1–7, https://doi.org/10.1155/2016/6208937.
11. Verma, C.; Ebenso, E.; Quraishi, M. Alkaloids as green and environmental benign corrosion inhibitors: An overview. *Int. J. Corros. Scale Inhib.* **2019**, *8*, 512–528, http://dx.doi.org/10.17675/2305-6894-2019-8-3-3.
12. Dohare, P.; Quraishi, M.; Verma, C.; Lgaz, H.; Salghi R.; Ebenso, E. Ultrasound induced green synthesis of pyrazolopyridines as novel corrosion inhibitors useful for industrial pickling process: experimental and theoretical approach. *Results Phys.* **2019**, *13*, 102344, http://dx.doi.org/10.1016/j.rinp.2019.102344.
13. Gonza´lez-Olvera, R.; Roma´n-Rodrı´guez, V.; Negro´n- Silva, G. E.; Espinoza-Va´zquez, A.; Rodrı´guez-Go´mez F. J..; Santillan, R. Multicomponent synthesis and evaluation of new 1, 2, 3-triazole derivatives of dihydropyrimidinones as acidic corrosion inhibitors for steel. *Molecules* **2016**, *21*, 250, https://doi.org/10.3390/molecules21020250.
14. Odewole, O. A.; Ibeji, C. U.; Oluwasola, H. O.; Oyeneyin, O. E.; Akpomie, K. G.; Ugwu, C. M.; Ugwu, C. G.; Bakare, T. E. Synthesis and anti-corrosive potential of Schiff bases derived 4-nitrocinnamaldehyde for mild steel in HCl medium: Experimental and DFT studies. *J. Mol. Struct.* **2021**, *1223*, 1–9, https://doi.org/10.1016/j.molstruc.2020.129214.
15. Ibrahim, M. A. A.; Moussa, N. A.M.; Mahmoud, A. H. M.; Sayed, S.R.M.; Sidhom, P. A.; Abd El-Rahman, M. K.; Shoeib T.; Mohamed, L. A. Density functional theory study of the corrosion inhibition performance of 6-mercaptopurine and 6-thioguanine expired drugs toward the aluminium (111) surface. *RSC Adv*. **2023**, *13*, 29023–29034, https://doi.org/10.1039/d3ra04954j.
16. Verma, C.; Ebenso, E. E.; Quraishi, M. A.; Hussain, C. M. Recent developments in sustainable corrosion inhibitors: design, performance and industrial scale applications. *Mater. Adv.* **2021**, *2*, 3806–3850, https://doi.org/10.1039/d0ma00681e.
17. Ogunyemi, B.T.; Ojo, F.K. Corrosion inhibition potential of thiosemicarbazide derivatives on aluminium: insight from molecular modelling and QSARs approaches. *J. Nig. Soc. Phys. Sci.* **2023**, *5*, 915, https://doi.org/10.46481/jnsps.2023.915.
18. Acharya, P. T.; Bhavsar, Z. A.; Jethava, D. J.; Patel, D. B.; Patel, D. H. A review on development of bio-active thiosemicarbazide derivatives: Recent advances. *J. Mol. Struct.* **2021**, *1226*, 129268, https://doi.org/10.1016/j.molstruc.2020.129268.
19. Gummanar, N.; Mokshanatha, P. B.; Dyapur, P.; Yallappa, G. N. Organic corrosion inhibitors for aluminum-based alloys –A Review. *Lett. NanoBioSci.* **2023**, *12*, 170, https://doi.org/10.33263/LIANBS124.170.
20. Obot, I. B.; Kaya, S.; Kaya, C.; Tuzun, B. Theoretical evaluation of triazine derivatives as steel corrosion inhibitors: DFT and Monte Carlo simulation approaches. *Res. Chem. Intermed.* **2015**, 1-20, https://doi.org/10.1007/s11164-015-2339-0.
21. Uzah. T.T., Mbonu, J. I., Gber, T. E. and Louis, H. Synergistic effect of KI and urea on the corrosion protection of mild steel in 0.5 M H_2SO_4: Experimental and computational insights. *Results. Chem.* **2023**, *5*, 1-9, https://doi.org/10.1016/j.rechem.2023.100981.
22. Ambrish, S.; Kashif, R.A.; Mumtaz, A.Q.; Yuanhua, L. Investigation of Corrosion Inhibitors Adsorption on Metals Using Density Functional Theory and Molecular Dynamics Simulation. In Corrosion Inhibitors, Ambrish, S., Ed.; IntechOpen: Rijeka, **2019**; p. Ch. 7, https://doi.org/10.5772/intechopen.84126.
23. Bourzi, H.; Oukhrib, R.; El Ibrahimi, B.; Oualid, H. A.; Abdellaoui, Y.; Balkard, B.; El Issami, S.; Hilali, M.; Bazzi, L.; Len, C. Furfural analogs as sustainable corrosion inhibitors—predictive efficiency using DFT and Monte Carlo simulations on the Cu(111), Fe(110), Al(111) and Sn(111) surfaces in acid media. *Sustainability* **2020**, *12*, 3304, https://doi.org/10.3390/su12083304.
24. Khabazi, M. E.; Chermahini, A. N. DFT study on corrosion inhibition by tetrazole derivatives: investigation of the substitution effect. *ACS Omega* **2023**, *8*, 9978−9994, https://doi.org/10.1021/acsomega.2c07185.
25. Guo, L.; Obot, I.B.; Zheng, X.; Shen, X.; Qiang, Y.; Kaya, S.; Kaya, C. Theoretical insight intoan empirical rule about organic corrosion inhibitors containing nitrogen, oxygen, and sulfur atoms, *Appl. Surf. Sci.* **2017**, *406*, 301–306, http://dx.doi.org/10.1016%2Fj.apsusc.2017.02.134.

26. Hadisaputra, S.; Purwoko, A. A.; Hakim, A.; Prasetyo, N.; Hamdiani S. Corrosion inhibition properties of phenyl phthalimide derivatives against carbon steel in the acidic medium: DFT, MP2, and Monte Carlo simulation studies. *ACS Omega* **2022**, *7*, 33054–33066, https://doi.org/10.1021/acsomega.2c03091.
27. Iorhuna, F.; Ayuba, A. M.; Nyijime A. T. Comparative study of skimmianine as an adsorptive inhibitor on Al (110) and Fe (111) crystal surface, using DFT and simulation method. *J. Chem. Lett*. **2023**, *4*, 148-155, https://doi.org/10.22034/JCHEMLETT.2023.398506.1117.
28. Fouda, A. S.; Etaiw, S. E. H; Ibrahim, A. M.; El-Hossianya, A. A. Insights into the use of two novel supramolecular compounds as corrosion inhibitors for stainless steel in a chloride environment: experimental as well as theoretical investigation. *RSC Adv*. **2023**, *13*, 35305–35320, https://doi.org/10.1039/d3ra07397a.
29. Uzah, T.T.; Mbonu, J.I. Enhancing the inhibition action of acetamide with iodide ions for mild steel corrosion in 0.5 M H_2SO_4 environment. *Lett. Appl. NanoBioSci.* **2024**, *13*, 1-16, https://doi.org/10.33263/LIANBS131.049.
30. Arrousse, N., Fernine, Y., Al-Zaqri, N., Boshaala, A., Ech-chihbi, E., Salim, R., El Hajjaji, F., Alami, A., Ebn Touhamie, M.; Taleba, M. Thiophene derivatives as corrosion inhibitors for 2024-T3 aluminum alloy in hydrochloric acid medium. *RSC Adv.* **2022**, *12*, 10321–10335, https://doi.org/10.1039/d2ra00185c.
31. Uzah, T. T.; Mbonu, I. J. Insight into synergistic corrosion inhibition of thiourea and $ZnCl_2$ on mild steel: Experimental and theoretical Approaches. *J. Chem. Lett.* **2023**, *4*, 211-221, https://doi.org/10.22034/jchemlett.2024.413932.1135.
32. Kaya, S.; Kaya, C. A new method for calculation of molecular hardness: A theoretical study, computational and theoretical chemistry **2015**, *1060*, 66, https://doi.org/10.1016/j.comptc.2015.03.004.
33. Thakur, A.; Kumar, A. Computational insights into the corrosion inhibition potential of some pyridine derivatives: A DFT approach. *Eur. J. Chem.* **2023**, *14*, 246-253, https://dx.doi.org/10.5155/eurjchem.14.2.246-253.2408.
34. Iorhunaa, F.; Nyijime, A. T.; Lawal. S. M. Theoretical properties of thiazepine and its derivatives on inhibition of aluminium Al (110) surface. *Alger. J. Eng. Technol*. **2023**, *1*, 43-51, https://doi.org/10.57056/ajet.v8i1.89.
35. Jabri, Z.; El Ibrahimi, B.; Jarmoni, K.; Sabir, S.; Misbahi, K.; Rodi, Y. K.; Mashrai, A.; Hökelek, T.; Mague, J. T.; Sebbar, N. K.; Essassi. E. New imidazo[4,5-b] pyridine derivatives: synthesis, crystal structures, hirshfeld surface analysis, DFT computations and Monte Carlo simulations. *J. Chem. Technol. Metallur* **2022**, *57*, 451-463.
36. Uzah T.T. DFT and Monte Carlo Simulation for the Prediction of Corrosion Inhibitive Efficacy of Selected Thiosemicarbazide Derivatives on Al (111) and Cu (111) Surfaces in Acidic Media. *J. Med. Nanomater. Chem.* **2024**, *6*, 81-94, https://doi.org/10.48309/JMNC.2024.1.7.
37. Benzidia, B.; Barbouchi, M.; Hsissou, R.; Zouarhi, M.; Erramli, H.; Hajjaji, N. A combined experimental and theoretical study of green corrosion inhibition of bronze B66 in 3% NaCl solution by Aloe saponaria (syn. Aloe maculata) tannin extract. *Curr. Res. Green. Sustain. Chem.* **2022**, *5*, 100299, https://doi.org/10.1016/j.crgsc.2022.100299.